Reaction $K^-p \to K^-p\pi^+\pi^-$ at 2.0 GeV/c*

P. M. Dauber,† P. E. Schlein, W. E. Slater, and H. K. Ticho

Department of Physics, University of California, Los Angeles, California

(Received 29 October 1966)

An analysis of the reaction $K^-p \to K^-p\pi^+\pi^-$ at 2.0-GeV/c incident momentum is presented. The total cross section for the reaction is 627±20 μb, based on 4519 events. The reaction is dominated by resonance production through several channels which overlap kinematically but do not appear to interfere substantially. A maximum-likelihood procedure was used to determine the production fractions, which for the major channels are 0.44±0.02 for $N^{*++}(1236)$, 0.145±0.02 for $Y^{*0}(1520)$, 0.10±0.03 for $N^{*+}(1688)$, and 0.20±0.02 for simultaneous $\bar{K}^{*0}N^{*0}$. Evidence is presented for the production of $Y^{*+}(1765)$ and its decay into $Y^{*0}(1520)$ as well as for production of $Y^{*+}(1660)$ with decay into $K^-p\pi^+$. A four-standard-deviation enhancement is present at a $K^-\pi^+$ invariant mass of 690 MeV. Angular correlation data are presented for the $N^{*++}K^-\pi^-$, $Y^{*0}\pi^+\pi^-$, and $\bar{K}^{*0}N^{*0}$ reaction channels. However, the difficulty of separating the various channels prevents a detailed study of the reaction dynamics.

I. INTRODUCTION

A STUDY has been made of the reaction

$$K^-p \to K^-p\pi^+\pi^- \qquad (1)$$

at an incident momentum of 2.0 GeV/c (2234-MeV total center-of-mass energy). Data on $K^-p \to \bar{K}N2\pi$ reactions have been previously presented for momenta between 1.2 and 1.7 GeV/c,[1] at 1.80 GeV/c,[2] 1.95 GeV/c,[3] 2.24 GeV/c,[4] 2.63 and 2.70 GeV/c,[5] and 3.0 GeV/c.[6]

In the analysis reported here it is found that reaction (1) proceeds through several resonant intermediate states with comparable partial cross sections. The reaction is a copious source of the $\bar{K}^*(891)$, $N^*(1236)$, and $Y^*(1520)$ resonances. There is also evidence for the production of $Y^*(1660)$, $Y^*(1765)$, and one or more N^* resonances in the vicinity of 1688 MeV. The total energy is well above threshold for simultaneous production of $\bar{K}^{*0}(891)$ and $N^{*0}(1236)$, but in contrast to the situation in $K^+p \to K^+p\pi^+\pi^-$,[7–10] which proceeds domi-

nantly through $K^{*0}N^{*++}$, the $\bar{K}^{*0}N^{*0}$ mode accounts for only ~20% of the cross section for reaction (1).

II. EXPERIMENTAL PROCEDURE

The data were obtained in an exposure of the Lawrence Radiation Laboratory 72-in. hydrogen bubble chamber to a two-stage electrostatically separated K^- beam[11]; 200 000 pictures were obtained at an incident momentum of 2.00 GeV/c with a total useful K^- track length of 7.5 events/μb. The momentum spread of the beam was about ±2% and the pion contamination, determined from the observed number of events of the type $\pi^-p \to \pi^-p\pi^+\pi^-$, was (1.4±0.3)%. The path length of K^- in the experiment was determined by a count of τ-like K^- decays in the film. A branching fraction of (5.9±0.1)% for 3-prong decays was used.[12]

The film was scanned twice for events with 4-prong topology; the presence or absence of kinking secondary tracks was ignored. This was done in order to minimize biases against small-angle or short-length $\Sigma^\pm$ decays, which were later extracted kinematically. The $\Sigma^\pm$ events were measured in parallel with the other 4-prong events; the analysis of these events will be reported elsewhere.[13] For nonkinking 4-prong events, as well as for the τ decays, the two-scan detection efficiency was ~99%.

Each measured event was required to fit the hypothesis of reaction (1) with χ^2 probability $\gtrsim 0.01$. Ambiguities with other hypotheses and track ambiguities within the category of reaction (1) were resolved by visually inspecting the bubble density of

* Work supported in part by the U. S. Atomic Energy Commission.

† This paper forms part of a dissertation submitted in partial fulfillment of the requirements for the degree of Doctor of Philosophy, University of California, Los Angeles, 1966.

[1] S. G. Wojcicki, M. H. Alston, and G. R. Kalbfleisch, Phys. Rev. 135, B495 (1964).

[2] E. Colton, (private communication).

[3] L. T. Smith, Ph.D. thesis, University of California, Los Angeles, 1965 (unpublished).

[4] G. W. London, R. R. Rau, N. P. Samios, S. S. Yamamoto, M. Goldberg, S. Lichtman, M. Primer, and J. Leitner, Phys. Rev. 143, 1034 (1966).

[5] M. Pripstein, J. R. Ficenec, R. I. Hulsizer, D. W. Mortara, W. P. Swanson, and W. P. Trower, in *Proceedings of the 12th Annual International Conference on High-Energy Physics, Dubna, 1964* (Atomizdat, Moscow, 1965), p. 638; M. Pripstein (private communication).

[6] J. Badier, M. Demoulin, J. Goldberg, B. Gregory, C. Pelletier, A. Rouge, M. Ville, R. Barloutaud, A. Leveque, C. Loudec, J. Meyer, P. Schlein, A. Verglas, D. J. Holthuizen, W. Hoogland, J. C. Kluyver, E. DeLijser, A. G. Tenner, Saclay Internal Report No. CEA-N532, April 1965 (unpublished).

[7] G. Goldhaber, W. Chinowsky, S. Goldhaber, W. Lee, and T. O'Halloran, Phys. Letters 6, 62 (1963).

[8] G. Goldhaber, J. Brown, I. Butterworth, S. Goldhaber, A. Hirata, J. Kadyk, B. Shen, and G. Trilling, Phys. Letters 18, 76 (1965).

[9] M. Ferro-Luzzi, R. George, Y. Goldschmidt-Clermont, V. P.

Henri, B. Jongejans, D. W. G. Leith, G. R. Lynch, F. Muller, and J. M. Perreau, Nuovo Cimento 39, 417 (1965).

[10] F. Grard, J. Debaisieu, J. Henghebaert, L. Pape, and R. Windmolders, in *Proceedings of the 12th International Conference on High-Energy Physics, Dubna, 1964* (Atomizdat, Moscow, 1965), p. 718.

[11] J. J. Murray, J. Button-Shafer, F. T. Shively, G. H. Trilling, J. A. Kadyk, A. Rittenberg, D. M. Siegel, J. S. Lindsey, and D. Merrill, Lawrence Radiation Laboratory Report No. UCRL-11426, 1964 (unpublished).

[12] See references in the compilation by A. H. Rosenfeld, A. Barbaro-Galtieri, W. H. Barkas, P. L. Bastien, J. Kirz, and M. Roos, Rev. Mod. Phys. 37, 633 (1965).

[13] W. E. Slater, P. M. Dauber, P. E. Schlein, D. H. Stork, and H. K. Ticho, Bull. Am. Phys. Soc. 10, 1196 (1965); and unpublished.
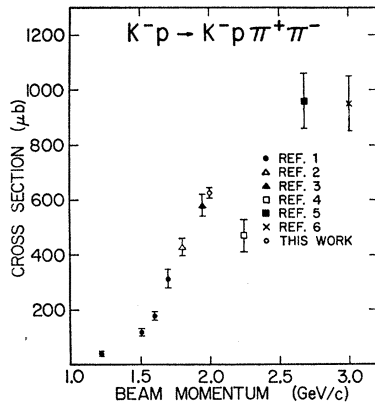
FIG. 1. Total cross section for the reaction $K^-p \to K^-p\pi^+\pi^-$ as a function of beam momentum.

the tracks. The laboratory momenta of the tracks were sufficiently small that virtually all such ambiguities could easily be resolved. The small contamination of pions in the beam and the small cross section for $K^-p \to K^-p\pi^+\pi^-\pi^0$ (6% of that for $K^-p\pi^+\pi^-$) at our energy permit a very pure sample of $K^-p \to K^-p\pi^+\pi^-$ to be obtained. In all, 4519 events of the latter type resulted from the measurements and satisfied fiducial-volume and beam-track requirements. The contamination due to all other reactions in this sample was estimated to be $(0.8\pm0.4)\%$ in a study of a subsample of the events.
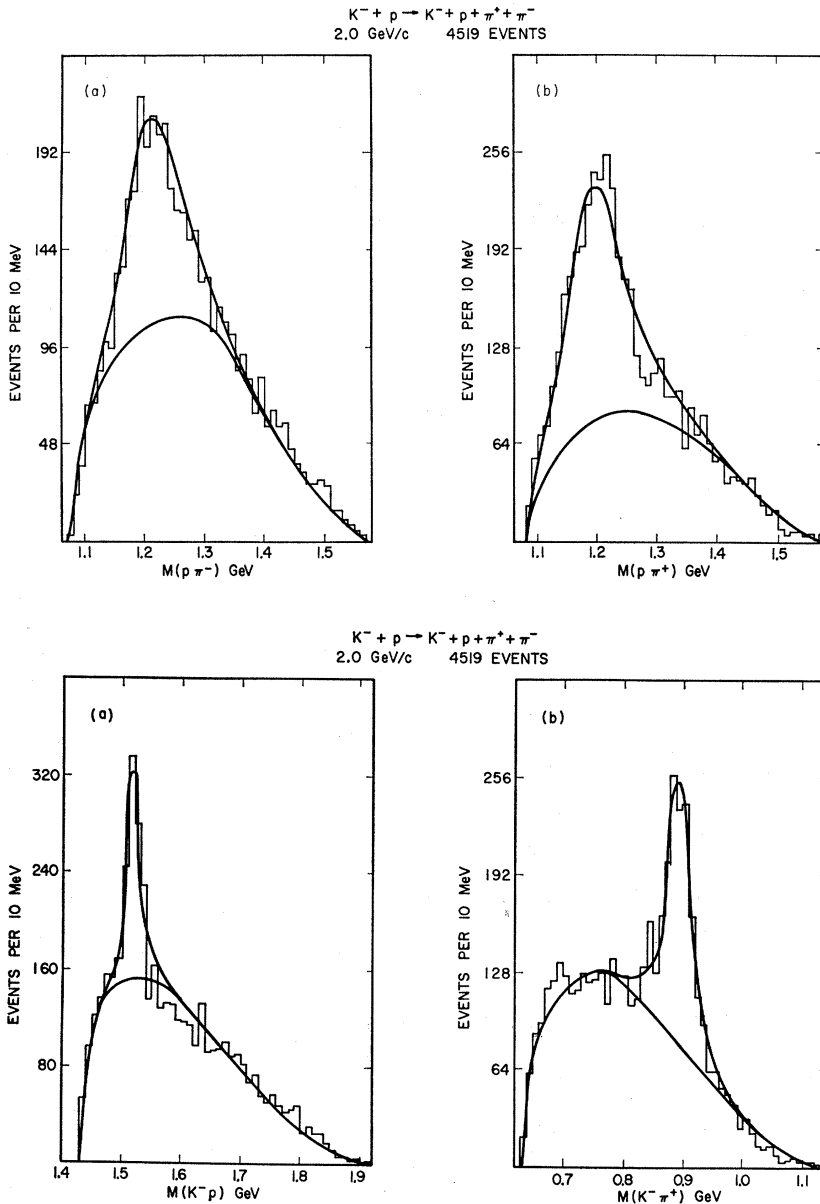

FIG. 2. Invariant mass spectra in the $K^-p\pi^+\pi^-$ final state. (a) $M(p\pi^-)$, (b) $M(p\pi^+)$. The curves were obtained by Monte Carlo using resonance fractions found in the maximum-likelihood fit.

FIG. 3. Invariant mass spectra in the $K^-p\pi^+\pi^-$ final state. (a) $M(K^-p)$, (b) $M(K^-\pi^+)$. The curves were obtained by Monte Carlo using resonance fractions found in the maximum-likelihood fit.

FIG. 4. Invariant mass spectra in the $K^-p\pi^+\pi^-$ final state. (a) $M(K^-\pi^-)$, (b) $M(\pi^+\pi^-)$. The curves were obtained by Monte Carlo using resonance fractions found in the maximum-likelihood fit.
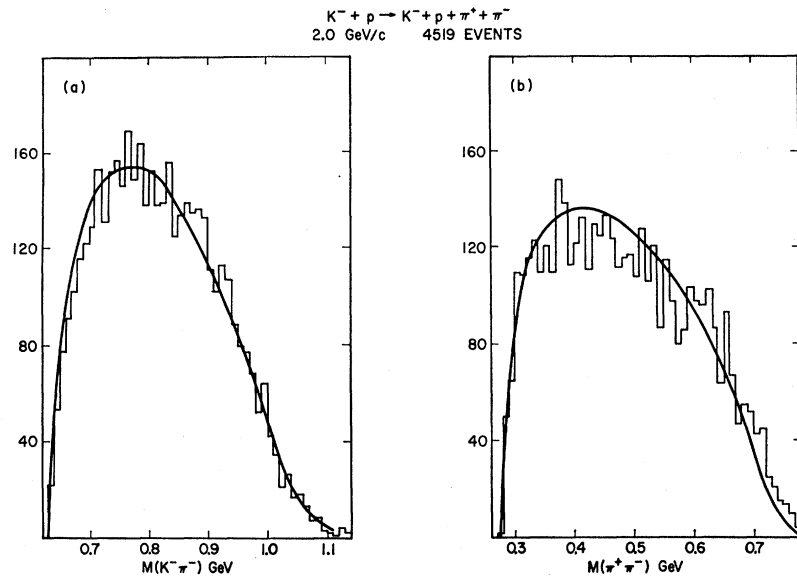
III. RESULTS AND DISCUSSION

A. Total Cross Section

The total cross section obtained for reaction (1) at 2.0 GeV/c is $\sigma = 627 \pm 20 \,\mu$b. This value includes a 6.5% net correction for lost and contaminant events. The error is due mainly to (a) the error in the path length, $\pm 2.6\%$, (b) the statistical uncertainty in the number of events, $\pm 1.5\%$ and (c) the uncertainty in the corrections for loss of events, $\pm 1.2\%$. At the lower momenta of 1.80 and 1.95 GeV/c, the cross sections are 430 ± 30 and $580 \pm 40 \,\mu$b, respectively.[2,3] Figure 1 shows

these cross sections along with those obtained in other experiments as a function of beam momentum.[1–6]

B. Analysis of Mass Spectra

Inspection of the invariant mass distributions of the 6 particle pairs and 4 triplets in the final state (Figs. 2–6) shows strong enhancements near the positions of $K^*(891)$ in $K^-\pi^+$, of $N^*(1236)$ in $p\pi^+$, and of $p\pi^-$ and $Y^{*0}(1520)$ in K^-p. There are no correspondingly large enhancements in the other mass distributions. In particular, there is no evidence for resonances in the

FIG. 5. Invariant mass spectra in the $K^-p\pi^+\pi^-$ final state. (a) $M(K^-p\pi^+)$, (b) $M(p\pi^+\pi^-)$. The curves were obtained by Monte Carlo using resonance fractions found in the maximum-likelihood fit.
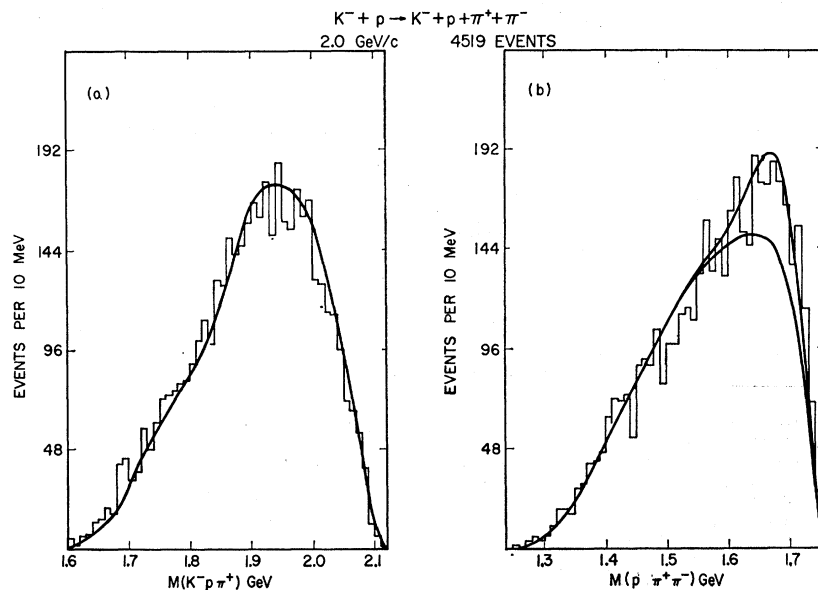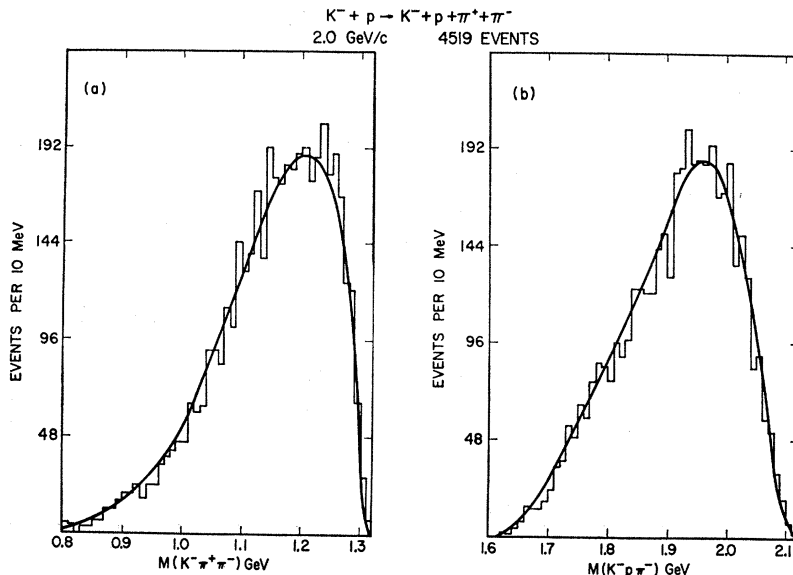
FIG. 6. Invariant mass spectra in the $K^- p \pi^+ \pi^-$ final state. (a) $M(K^- \pi^+ \pi^-)$, (b) $M(K^- p \pi^-)$. The curves were obtained by Monte Carlo using resonance fractions found in the maximum-likelihood fit.

$K^- \pi^+ \pi^-$ or $\bar{K}^* \pi^-$ systems in the mass range of 1.1–1.3 GeV where enhancements have been reported.[14] Inspection of the scatter diagram of $K^- \pi^+$ mass vs $p \pi^-$ mass (Fig. 7) reveals a concentration of events in the region where the $\bar{K}^{*0}$ and N^{*0} bands cross. The size
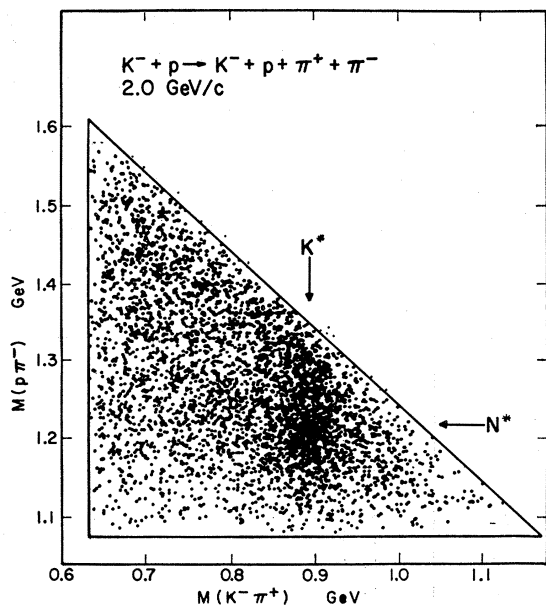

FIG. 7. Scatter diagram of $(p\pi^-)$ vs $(K^-\pi^+)$ invariant mass in the $K^- p \pi^+ \pi^-$ final state.

[14] R. Armenteros, D. N. Edwards, T. Jacobsen, L. Montanet, A. Shapira, J. Vandermeulen, Ch. D'Andlau, A. Astier, P. Baillon, J. Cohen-Ganouna, C. Defoix, J. Siaud, C. Ghesquiere, and P. Rivet, Phys. Letters 9, 207 (1964); T. P. Wangler, A. R. Erwin, and W. D. Walker, ibid. 9, 71 (1964); R. Bock, B. R. French, J. B. Kinson, V. Simak, J. Badier, M. Bazin, B. Equer, A. Rouge, and P. Grieve, ibid. 12, 65 (1964); J. M. Bishop, A. T. Goshaw, A. R. Erwin, M. A. Thomson, W. D. Walker, and A. Weinberg, Phys. Rev. Letters 16, 1069 (1966).

of these enhancements indicates that the $K^- p \pi^+ \pi^-$ reaction is dominated by single-resonance production as well as simultaneous $\bar{K}^{*0} N^{*0}$ production.

The mass spectra were fitted with a likelihood function which assumes a set of Breit-Wigner resonant amplitudes plus a phase space-like background. Interference between the amplitudes was neglected in constructing the likelihood function. This technique was first used by Friedman and Ross[15]; it provides a determination of the relative intensities of the major channels, which in turn permits kinematic reflections of all the peaks to be taken into account when fitted curves are drawn. Minor resonant channels may then show up as deviations from the curves. The likelihood function has the form

$$L = \prod_{j=1}^{N} \left(\sum_{i=1}^{n} \frac{f_j}{N_{ij}} |T_j|^2 \rho_i \right), \qquad (2)$$

where $N = 4519$ is the number of events, n is the number of processes, f_j is the branching fraction for the jth process, and ρ_i is the total phase space, subscripted because events with different beam momentum have different total phase space. For production according to pure phase space, $|T_j|^2 = 1$. For production of a resonance, the relativistic Breit-Wigner function[16]

$$|T_j|^2 = \frac{M\Gamma(M)}{q} \frac{q_0 \Gamma_0 M_0}{(M_0^2 - M^2)^2 + [M_0 \Gamma(M)]^2} \qquad (3)$$

was used to describe the dependence of the matrix element on the invariant mass M of the decay products. Here M_0 and Γ_0 are the resonant mass and the width of the resonant state, q_0 and q are the decay momenta for

[15] J. Friedman and R. Ross, Alvarez Group Programmers Note P-102, 1964 (unpublished).
[16] J. D. Jackson, Nuovo Cimento 34, 1644 (1964).

a decay at a mass M_0 and M, respectively, into two daughter products of the resonance. The dependence of the width on mass was taken to be

$$\Gamma(M) = \Gamma_0 C(q/q_0)^{2l+1}, \quad (4)$$

where the orbital angular momentum of the decay is $l=1$ for K^* and N^* and $l=2$ for $Y^{*0}(1520)$. An empirical correction factor[16]

$$C = (am_\pi{}^2 + q_0{}^2)/(am_\pi{}^2 + q^2), \quad (5)$$

with $a=1$, was used in the N^* case to take the radius of interaction into account; otherwise $C=1$.

The normalization integrals

$$N_{ij} = \int |T_j|^2 \rho_i dM_j d\Omega_j \quad (6)$$

were evaluated numerically and $W = -\log L$ was minimized as a function of the fractions f_j on an IBM 7094 computer using the search routine MINFUN.[17] The presence of background as well as properties of the production mechanism of a given resonance may cause the experimental mass and width to be shifted from their established values. Therefore, empirical values of M_0 and Γ_0 were obtained from the data for the K^*, N^*, and Y^{*0} resonances. Because of the very large number of events, it proved computationally impractical to simultaneously minimize W with respect to the M_0 and Γ_0 of each resonance as well as with respect to the f_j. Thus, the M_0 and Γ_0 were determined by an approximation procedure in which only one mass or width was varied at a time. Table I contains the values obtained along with the values of M at maximum intensity (in general, less than M_0), the full width at half-maximum (FWHM) intensity and accepted[12] values of M_0 and Γ_0. It must be noted that the arbitrariness of the correction factor C in fitting the N^* implies a certain arbitrariness in the measured $\Gamma_0(N^*)$.

The Y^{*0} parameters obtained are in good agreement with the accepted values. On the other hand, the K^* mass obtained is somewhat higher and the corresponding width smaller than usually reported. Presumably, the observed 20-MeV mass difference between N^{*0} and N^{*++} is associated primarily with differences in the production mechanism of the two charge states.[18]

The masses and widths presented in Table I were used in the likelihood fit to the mass spectra which assumed the seven channels tabulated in Table II.

[17] W. E. Humphrey, Alvarez Group Programmers Note P-6, 1962 (unpublished).

[18] The N^{*++} and N^{*0} peak positions are substantially the same as in the $K^-p \to K3p\pi^+\pi^-$ reaction at 2.7 GeV/c [M. Pripstein (private communication)]. In $K^+p \to K^+p\pi^+\pi^-$ at 3 GeV/c, the N^{*++} position is reported as $M_0 = 1220 \pm 6$ MeV (Ref. 9). In $\pi^-p \to \pi^-p\pi^+\pi^-$ at 2.7 GeV/c, the N^{*++} "central value" is reported as 1210 MeV while that for N^{*0} is given as 1230 MeV [P. Klein et al., 1965 Athens Conference (unpublished)]. Thus, the lowering of the N^{*++} mass appears to be a common occurrence in multiparticle final states.

TABLE I. Parameters of K^*, N^* and Y^{*0} resonances in $K^-p \to K^-p\pi^+\pi$ at 2.0 GeV/c.

Reso-nance	M_0 (MeV)	Accepted[a] M_0	M_{peak}	Γ_0 (MeV)	Accepted[a] Γ_0	FWHM[c]
K^*	894.7 ± 1.3	891.4 ± 0.8	892.5	44 ± 4	49 ± 2	44
N^{*0}	1235 ± 3	1236.0 ± 0.4	1214	145 ± 7[b]	120.0 ± 1.5	120
N^{*++}	1215 ± 2	1236.0 ± 0.4	1191	145 ± 7[b]	120.0 ± 1.5	112
Y^{*0}	1518 ± 1	1518.9 ± 1.5	1517	16 ± 2	16 ± 2	15

[a] See Ref. 12.
[b] These were constrained to be equal.
[c] Full width at half-maximum intensity of resonance.

Branching fractions f_j and partial cross sections are presented for each channel. The hypothesis of simultaneous $\bar{K}^{*0}$ and N^{*0} production was simulated by multiplying the Breit–Wigner intensities for $\bar{K}^{*0}$ and N^{*0}, i.e.,

$$|T_{\bar{K}^{*0}N^{*0}}|^2 = |T_{\bar{K}^{*0}}|^2 \times |T_{N^{*0}}|^2. \quad (7)$$

It was necessary to include the $N^*(1688)$ channel because, as may be noted in Fig. 5(b), the $p\pi^+\pi^-$ mass distribution is peaked at high mass. A run without the $N^*(1688)$ channel yielded a poor fit in this region, the discrepancy being about 3 standard deviations. For this channel, $M_0 = 1688$ MeV and $\Gamma_0 = 100$ MeV[12] with a simple $(\Gamma = \Gamma_0)$ Breit-Wigner shape were used. The errors in Table II were obtained in the usual way by inverting the second derivative matrix of χ^2 (calculated by numerical differentiation) and taking the square root of the diagonal elements. Monte Carlo studies[3] have indicated that this procedure results in errors which may be interpreted as standard deviations.

The curves in Figs. 2–6 are the distributions of Monte Carlo events generated according to phase space and the resonant shapes (3), normalized to the number of physical events and smoothed out to eliminate statistical fluctuations. The background curve under each resonant peak was obtained by plotting all the Monte Carlo events except those in channels in which the resonance is produced. It will be noted that the curves in Figs. 2–6 are generally adequate representations of the data. Discrepancies between the experimental distributions and the fitted curves may indicate low-intensity channels which have been overlooked;

TABLE II. Branching fractions and cross sections for production channels in $K^-p \to K^-p\pi^+\pi^-$ at 2.0 GeV/c.

Channel	Fraction (%)	Partial[a] cross section (μb)
$\bar{K}^{*0}p\pi^-$	3 ± 2	21 ± 11
$N^{*0}K^-\pi^+$	6 ± 2	36 ± 11
$\bar{K}^{*0}N^{*0}$	20 ± 2	125 ± 11
$N^{*++}K^-\pi^-$	44 ± 2	275 ± 15
$Y^{*0}\pi^+\pi^-$	13 ± 2	82 ± 13[b]
$N_{1/2}^*(1688)K^-$	10 ± 3	63 ± 19
Background	<4	<25
Total		627 ± 20

[a] The cross sections refer only to decay modes which result in the $K^-p\pi^+\pi^-$ final state.
[b] This cross section does not include the 9 ± 3-μb contribution of the $Y^*(1765) \to Y^*(1520)$ channel discussed in Sec. IIID.

they may also result from interference effects or reflections of angular correlations in the production and decay of the resonant states. Such correlations were not included in the likelihood function; they are not expected to be important because, as will be seen below, the production and decay distributions measured in the experiment are generally rather flat. Interference effects would be expected to show up more clearly where resonant bands cross on the various mass scatter plots. The plots for each pair of resonances were compared to similar plots of the Monte Carlo events generated according to the assumption of incoherence. No significant enhancements or depletions were observed. In general, the assumption of incoherent superposition of resonant channels seems well borne out by the data.

C. Production-Angle Moments as a Function of Invariant Mass

The production angular distributions of the various invariant-mass combinations may be represented by the moments of Legendre polynomials $\langle P_1 \rangle$, $\langle P_2 \rangle$, etc.,
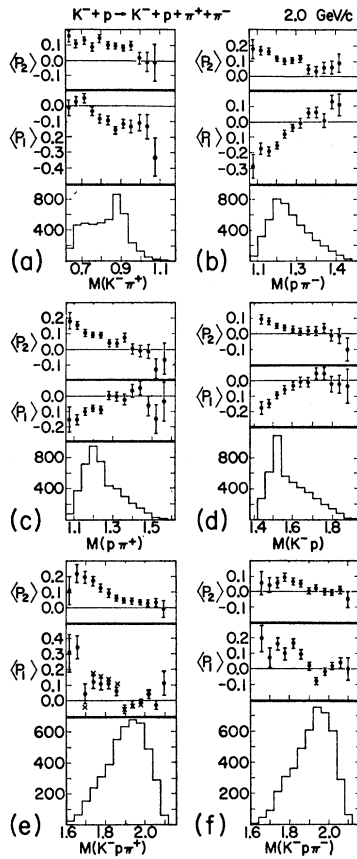

(a) (b) (c) (d) (e) (f)

FIG. 8. Production-angle moments of Legendre polynomials as a function of the invariant mass of the produced system. The mass combinations plotted are (a) $K^-\pi^+$, (b) $p\pi^-$, both using the $p\pi^-$ production angle; (c) $p\pi^+$, (d) K^-p; and (e) $K^-p\pi^+$, (f) $K^-p\pi^-$, both using the angle of the pion recoiling against the three-particle system. The crosses in (e) show the effect of the selection $1.50 < M(K^-p) < 1.54$ GeV.

of the production angle. Variations in these moments with invariant mass may suggest changes in the production mechanism at a particular mass value, such as peripheral resonance production. The alternative approach of plotting angular distributions for selected mass intervals is employed in later sections. There are 6 doublet and 4 triplet mass combinations available and 7 center-of-mass production angles associated with them (3 mass combination pairs have one production angle each). Figures 8(a) through (f) shows these moments as a function of $K^-\pi^+$, $p\pi^-$, $p\pi^+$, K^-p, $K^-p\pi^+$, and $K^-p\pi^-$ mass, respectively. The $p\pi^-$ production angle has been used in both (a) and (b); (c) and (d) are presented in terms of the $p\pi^+$ and K^-p angles, respectively. The moments in (e) and (f) are based on the π^- and π^+ production angles. It was found that most distributions are adequately characterized by $\langle P_1 \rangle$ and $\langle P_2 \rangle$ alone. $\langle P_3 \rangle$ is usually small and very slowly varying with mass.

Plots (a) and (b) indicate that the $p\pi^-$ system is produced relatively backward for $M(K^-\pi^+) \sim M_{K^*}$ and $M(p\pi^-) \sim M_{N^*}$. Plots (c) and (d) show a variation of $\langle P_1 \rangle$ and $\langle P_2 \rangle$ similar to that in plot (b); $\langle P_1 \rangle$ increases while $\langle P_2 \rangle$ decreases with increasing proton+meson invariant mass. Most striking perhaps is the absence of a major change in the behavior of these moments near resonant mass values, in particular as the K^-p mass passes through the very pronounced $Y^{*0}(1520)$ resonance in plot (d).

In contrast to the above, plot (e) shows significant variation of the $K^-p\pi^+$ production moment. Near $M(K^-p\pi^+) = 1660$ MeV, a large $\langle P_1 \rangle \sim 0.3$ is observed. Throughout the region near 1.8 GeV, $\langle P_1 \rangle$ is also positive and ~ 0.1. If only events with $1.50 < M(K^-p) < 1.54$ GeV are selected, $\langle P_1 \rangle$ is even more positive, as shown by the crosses in plot (e). Evidence will be presented below for $Y^{*+}(1765)$ in this mass region decaying to $Y^{*0}(1520)$, as well as for peripheral production of $Y^{*+}(1660)$. Above 1860 MeV, $\langle P_1 \rangle$ seems consistent with zero. Plot (f) displays a four-standard-deviation negative $\langle P_1 \rangle$ in the 40-MeV bin centered at $M(K^-p\pi^-) = 1940$ MeV; elsewhere $\langle P_1 \rangle$ is positive or consistent with zero. This behavior is suggestive of forward production of a narrow Y^{*-} resonance, but the data are insufficient to provide additional evidence for such an effect.

D. Small Resonant Channels

The possibility of resonances in the $K^-p\pi^+$ and $K^-p\pi^-$ systems is now considered. The $\langle P_1 \rangle$ production moment displays a rapid variation for the $K^-p\pi^+$ system. Furthermore, there is a small, narrow enhancement above the fitted curve just below 1700 MeV in $K^-p\pi^+$ mass [Fig. 5(a)] and a slight excess of events in the region just below 1800 MeV. To enhance these effects, events (mostly K^*) with $0.84 < M(K^-\pi^+) < 0.94$ GeV were removed and $K^-p\pi^+$ mass was plotted in

Fig. 9 for regions in K^-p mass below, at, and above the $Y^{*0}(1520)$ position. These selections favor low $K^-p\pi^+$ mass and erect a kinematic peak, as shown in each of the plots (a), (b), and (c) in Fig. 9 by the dotted Monte Carlo curves. These curves are the result of making the same mass selections on the Monte-Carlo events as on the real events; they are normalized to the total number of events in each of the three plots, (a), (b), and (c).[19] Plot (b), which contains mostly $Y^{*0}(1520)$ events, shows an enhancement above the dotted curve near 1765 MeV, while plots (a) and (c) do not show this enhancement. This suggests the production of $Y^{*+}(1765)$ and its decay into $Y^{*0}(1520)$:

$$K^- + p \to Y^{*+}(1765) + \pi^-$$
$$\searrow$$
$$Y^{*0}(1520) + \pi^+$$
$$\searrow$$
$$K^- + p. \qquad (8)$$
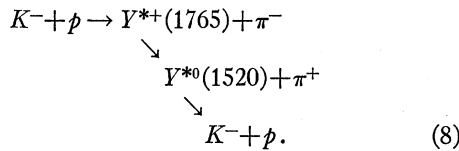
The decay of $Y_1^*(1765)$ into $Y^{*0}(1520)$ has been observed previously[20] in the s channel. This study, based on the $\Sigma^\pm \pi^\mp \pi^0$ final state, yielded $M(Y^*) = (1755 \pm 10)$ MeV, $\Gamma = (105 \pm 20)$ MeV, $J^P = \frac{5}{2}^-$ and a branching fraction for $Y^*(1765)$ decaying to $Y^*(1520)$ of 0.15 ± 0.03. Earlier results[21] suggested a slightly higher mass, $M = (1765 \pm 10)$ MeV and somewhat smaller width, $\Gamma = (60 \pm 10)$ MeV. Within statistics, both the position and width of the excess seen in Fig. 9(b) are in accord with the above results.

Normalizing the Monte Carlo curve to the background regions [i.e., excluding the 4 bins of enhancement in Fig. 9(b)], as shown by the solid curve, yields a cross section of 8 ± 3 μb for the decay sequence (8). Correction for $Y^{*0}(1520)$ events outside of the region $1.50 < M(K^-p) < 1.54$ GeV and for events removed by the $M(K^-\pi^+)$ cut increases the cross section to 9 ± 3 μb. The latter value corresponds to a $Y^{*+}(1765)$ π^- production cross section of 0.41 ± 0.18 mb, when account is taken of decaying branching factors.[12,20] Unfortunately, the very high background level in Fig. 9(b) precludes a more detailed analysis of this channel.

In Fig. 9(a), for $M(K^-p) < 1490$ MeV, the fit is reasonable near 1765 MeV but low below 1700 MeV. As shown in the subplot above plot (a), where events with forward going π^- are selected, the enhancement below 1700 MeV takes the form of a clear and narrow peak. This peak is centered at about 1670 MeV with a width

[19] This normalization differs from the over-all normalization of the Monte-Carlo events to all the real events by $+18$, -9, and $+18\%$ for (a), (b), and (c), respectively. The differences are due primarily to the rather poor fit of the Monte-Carlo curve to the $M(K^-p)$ distribution [Fig. 3(a)] in the $Y^*(1520)$ region and to other imperfections of the fit. These imperfections are expected to be only slightly reflected in the $M(K^-p\pi^+)$ distributions.

[20] R. Armenteros, M. Ferro-Luzzi, D. W. G. Leith, R. Levi Setti, A. Minten, R. D. Tripp, H. Filthuth, V. Hepp, E. Kluge, H. Schneider, R. Barloutaud, P. Granet, J. Meyer, and J. P. Porte, Phys. Letters **19**, 338 (1965).

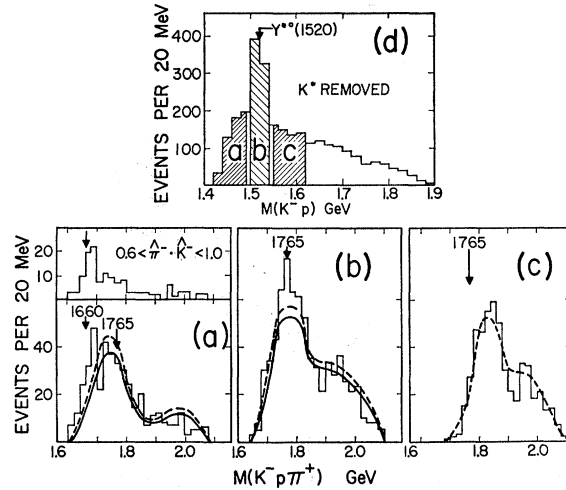[21] A. Barbaro-Galtieri, A. Hussain, and R. D. Tripp, Phys. Letters **6**, 296 (1963).

FIG. 9. Distributions of $K^-p\pi^+$ invariant mass for the intervals of K^-p mass shown in plot (d). (a) 1.40–1.49 GeV, (b) 1.50–1.54 GeV, and (c) 1.55–1.62 GeV. Events with $0.84 < M(K^-\pi^+) < 0.94$ GeV have been removed. The dashed curves were obtained by Monte Carlo from the fit to the major channels, and are normalized to the number of events in each of the three plots. The solid curves in (a) and (b) show the result of renormalizing to the events outside the regions of Y_1^* enhancement. The subplot above plot (a) shows $M(K^-p\pi^+)$ for the events in plot (a) satisfying $0.6 < \hat{\pi}^- \cdot \hat{K}^- \leqslant 1.0$.

of about 40 MeV. These results agree with the accepted parameters[12] for the $Y_1^*(1660)$, $M = (1660 \pm 10)$ MeV, and $\Gamma = (44 \pm 5)$ MeV. Normalizing the fit in Fig. 9(a) to the events outside the region of enhancement yields 63 ± 12 as the number of events above background or a cross section of 9 ± 2 μb for the process

$$K^- + p \to Y^{*+}(1660) + \pi^-$$
$$\searrow$$
$$K^- + p + \pi^+. \qquad (9)$$
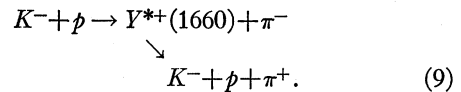
The production angular distribution of the events in the peak region is highly peripheral, as indicated by the moment plot of Fig. 8(e).

The analysis of the mass spectra did not yield substantial evidence for other Y_1^* effects. In particular, there is no evidence for the decay of $Y^*(1765)$ to $N^{*++} + K^-$. To check this possibility, events were selected in the N^{*++} mass band but outside a 40-MeV-wide $Y^{*0}(1520)$ band. The resulting $M(K^-p\pi^+)$ distribution shows no enhancement in the region below 1800 MeV. There is also no evidence of $Y^{*-}(1765)$ or $Y^{*-}(1660)$.

E. Low Mass Enhancement in the $K^-\pi^+$ Spectrum

The $K^-\pi^+$ mass distribution, Fig. 3(b), shows a small enhancement above the Monte Carlo curve at $M(K^-\pi^+) \cong 690$ MeV. Quantitatively, there is an excess of 75 ± 25 events (~ 10 μb) between 670 and 710 MeV. Similar enhancements have been observed in the same reaction at 1.80 and 1.95 GeV/c.[2,3] Our enhancement is centered at a mass substantially below that reported
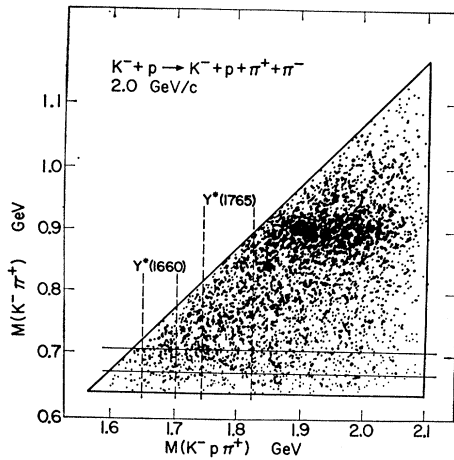
FIG. 10. Scatter diagram of $M(K^-\pi^+)$ versus $M(K^-p\pi^+)$. The dashed vertical bands show the regions of enhancement due to production of $Y_1^*(1660)$ and $Y_1^*(1765)$, while the solid horizontal band shows the enhanced interval of $K^-\pi^+$ mass.

for the effect known as the kappa meson. The κ has been seen in $\pi^-p \to \Sigma(\Lambda)\pi K$,[22] in $K^-p \to \bar{K}^0\pi^-p$,[23] and $\Xi K\pi$,[4] as well as $K^+p \to KN3\pi$.[24] The reported masses are consistent; their average is 725 ± 2 MeV[12] while widths $\Gamma \lesssim 20$, <12, <15, and <30 MeV were quoted in these experiments. In general, the status of κ as a meson is in some doubt due to its appearance in relatively few reactions. We shall discuss our own enhancement in greater detail below and explore possible explanations for its existence.

The enhancement at $M(K^-\pi^+) \sim 690$ MeV is associated with low $M(K^-p\pi^+)$. Figure 10 shows the scatter diagram of these masses with dotted bands corresponding to the small $Y_1^*(1660)$ and $Y_1^*(1765)$ enhancements discussed above. A projection of this scatter diagram onto the $M(K^-\pi^+)$ axis for the selection $M(K^-p\pi^+)$ <1.8 GeV is shown in Fig. 11(b). This selection serves to enhance the effect; in fact, essentially the entire enhancement is retained in the $M(K^-p\pi^+)<1.8$ GeV/c plot. Normalization of the Monte Carlo curve (based on the fit to the major channels) to the unenhanced bins results in a total of 67 ± 16 events above expectation. The band of $M(K^-\pi^+)$ enhancement, 40 MeV in width, is shown on the scatter diagram of Fig. 10. Figure 11(a) shows $M(K^-p\pi^+)$ for events in the band of $M(K^-\pi^+)$ enhancement with the curve normalized to the total number of events. The excess below 1.8 GeV corresponds to about 50 of the 125 total Y_1^* events, a result expected if the Y_1^* events are roughly uniformly distributed in $M(K^-\pi^+)$. Thus, the $M(K^-\pi^+)$ enhancement is not a kinematic reflection of the Y_1^* resonances.

Conceivably, the $K\pi$ peak could arise from an interference effect, possibly one involving the Y_1^*'s and a "background" amplitude such as that for N^{*++}, which is important in this mass region. Another possibility involving the N^{*++} is provided by the existence of singularities in triangle diagrams such as that shown in Fig. 12.

Coleman and Norton[25] have shown that the singularity in $s=M(K^-\pi^+)$ occurs for physical values of s if and only if the diagram can be interpreted as a classical (on-the-mass-shell) process in space-time. The π^+ from the N^{*++} decay must actually be able to catch and scatter off the K^-. For point particles, this condition requires the N^{*++} to decay such that the π^+ is emitted opposite to the N^* direction of motion and sets limits on s and $W=M(K^-p\pi^+)$ within which the rescattering can occur. For a given N^{*++} mass, the value of s at which the singularity occurs decreases with increasing W from its maximum at $N^{*++}K^-$ threshold ($s=730$ MeV for $M_{N^*}=1236$ MeV) to $s=M_K+M_\pi=633.4$ MeV at that value of W for which the kaon and pion velocities are equal. The observed $K\pi$ enhancement lies within the required kinematic region. Furthermore, for W near $N^{*++}K^-$ threshold, the distances which must be traveled by the K^- and π^+ are a few Fermis, so that the solid angle for rescattering is large. In fact, W for our
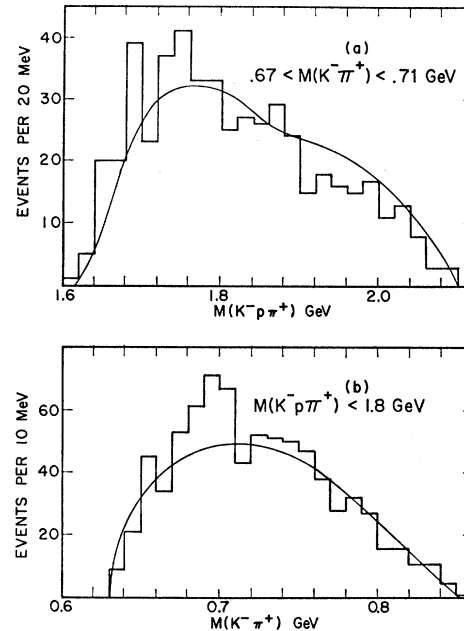

FIG. 11. (a) Distribution of $M(K^-p\pi^+)$ for events satisfying $0.67<M(K^-\pi^+)<0.71$ GeV. The curve was obtained by Monte Carlo from the fit to the major channels (excluding the charged Y^* channels) and is normalized to the total number of events in the plot. (b) Distribution of $M(K^-\pi^+)$ for events satisfying $M(K^-p\pi^+)<1.8$ GeV. The curve is normalized to the total number of events in the plot.

[22] D. H. Miller, G. Alexander, O. I. Dahl, L. Jacobs, G. R. Kalbfleisch, and G. A. Smith, Phys. Letters 5, 279 (1963).
[23] S. G. Wojcicki, G. R. Kalbfleisch, and M. H. Alston, Phys. Letters 5, 283 (1963).
[24] M. Ferro-Luzzi, R. George, Y. Goldschmidt-Clermont, V. P. Henri, B. Jongejans, D. W. G. Leith, G. R. Lynch, F. Muller, and J. M. Perreau, Phys. Letters 12, 255 (1964).

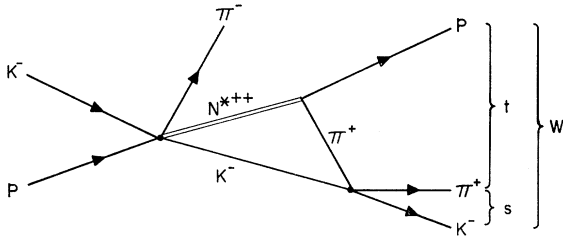[25] S. Coleman and R. E. Norton, Nuovo Cimento 38, 438 (1965).

FIG. 12. Triangle diagram for $K^- p \to K^- p \pi^+ \pi^-$ with N^{*++} as an internal line.

enhancement varies between 1.6 and 1.8 GeV while the $N^* K$ threshold is 1.7 GeV for N^* events at the central mass. Finally, the resonance production diagram, i.e., Fig. 12 without the rescattering, is important; $N^{*++} K^- \pi^-$ is the largest reaction channel in the $K^- p \pi^+ \pi^-$ final state. The $Y^{*0}(1520)$ channel is also large; however, the rescattering in that case occurs only for $s < 647$ MeV, which is below our peak.

Several authors[26–28] have calculated enhancements arising from the triangle mechanism; the diagram without rescattering was regarded as background in these papers. Schmid[29] has pointed out, however, that the resonance-production diagram also has singularities which are of the same form and occur at the same energy as those of the triangle diagram. When the singular parts of each diagram are added coherently, the net result of the rescattering diagram is merely a multiplication of the amplitude for the resonance production diagram by a phase factor. On a plot of s^2 versus t^2, where $t = M(p\pi^+)$ (for fixed W this is a Dalitz plot), the rescattering has the effect of removing events from the low-s end of the resonance band and redistributing them in t. Thus, a projection of the Dalitz plot onto s shows a peak only if events in the resonance band are not included; the projection for all events does not show an enhancement in contrast to the effect reported above. This result is not surprising; classically, an elastic scattering does not change s. There may be a way of overcoming the objection raised by Schmidt. The large and energy-dependent width[30] of the N^{*++} or the fact that all three vertices of the triangle diagram lie within a small interaction volume (radius $\sim 1F$) for much of the enhancement region may alter his analysis so as to permit enhancement.

F. Production and Decay of N^{*++} and Y^{*0}

The strongest channel leading to the $K^- p \pi^+ \pi^-$ final state is

$$K^- + p \to N^{*++} + K^- + \pi^- , \qquad (10)$$

[26] Y. F. Chang and S. F. Tuan, Phys. Rev. **136**, B741 (1964).
[27] F. R. Halpern and H. L. Watson, Phys. Rev. **131**, 2674 (1963).
[28] M. Month, Phys. Rev. **139**, B1093 (1965).
[29] C. Schmid, Massachusetts Institute of Technology (unpublished).
[30] In general, the effect of giving the N^* mass an imaginary part to account for its width is to move the singularity *away* from the physical region (i.e., real s) so that it is by no means clear how

with no intermediate two-body state. Although reaction (10) is a three-body reaction, one may study the relevant angular correlations in the hope of finding effects characteristic of a simple production mechanism. The N^{*++} mass band is defined by $1.13 < M(p\pi^+) < 1.27$ GeV. According to the Monte-Carlo calculation, this sample of events contains 60% N^{*++}. When most of the $\bar{K}^*$ and $Y^{*0}(1520)$ events are eliminated by removing events which satisfy either $0.86 < M(K^- \pi^+)$ < 0.92 GeV or $1.50 < M(K^- p) < 1.54$ GeV, or both, the remaining purified sample contains $\sim 71\%$ N^{*++}. However, 400 of the 1550 N^{*++} events in the N^* mass band are lost by the cuts.

The c.m. production angular distribution of the $p\pi^+$ system is shown in Fig. 13(a) for the 71% N^* selection; the distribution of squared four-momentum transfer between target proton and N^{*++} is presented in Fig. 13(b). The sharp backward peak in the angular distribution is washed out when Δ^2 is used. This effect may be ascribed to the width of the N^* and the variable mass of the $K^- \pi^-$ system recoiling against the N^{*++}. The possibility that the peak in the production cosine is associated with a peripheral mechanism can be investigated further by a study of the decay correlations of the N^{*++}. Figure 14 shows the distribution of N^{*++} decay for both the 60% and the 71% N^* samples. The angles whose cosines are plotted are θ_{target}, the angle between the target and decay protons in the N^{*++} rest frame and θ_{normal}, the angle between the decay proton and the direction $\hat{K}^-_{\text{in}} \times \hat{N}^{*++}$. The distribution of $\cos\theta_{\text{target}}$ in (a) is peaked in the forward direction (the decay proton is emitted backward in the c.m. system); much of this asymmetry disappears when K^* and Y^* events are removed; see Fig. 14(b). This distribution is
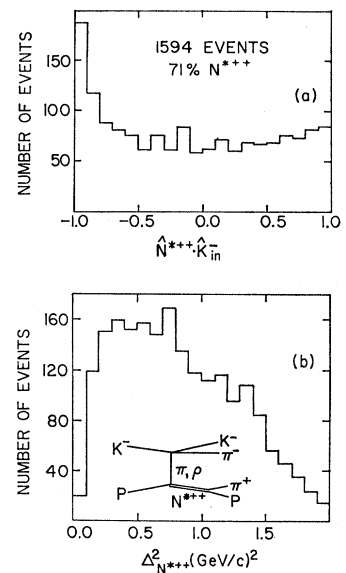
FIG. 13. (a) Production angular distribution of N^{*++} in the reaction $K^- p \to N^{*++} K^- \pi^-$. (b) Distribution of squared momentum transfer to the N^{*++}. The diagram shown is the one-meson-exchange diagram for which the N^{*++} is produced alone at the lower vertex.

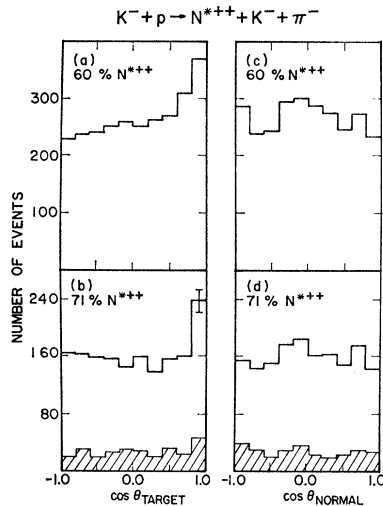the large width of the N^* can help to produce an enhancement [R. E. Norton (private communication)].

$$K^- + p \to N^{*++} + K^- + \pi^-$$

FIG. 14. Decay angular distributions of the N^{*++} system with respect to the target proton and normal $(\hat{K}^- \times \hat{N}^{*++})$ directions (see text). Plots (a) and (c) show events in the N^{*++} mass band; events in the $\bar{K}^*$ and $Y^*(1520)$ bands were also removed in plotting (b) and (d). The cross-hatched histograms in (b) and (d) show the events in the interval $\hat{N}^{*++} \cdot \hat{K}^- < -0.8$.

flat except for a small forward peak; the distribution of $\cos\theta_{normal}$ in Fig. 14(d) is consistent with isotropy. The decay distributions in (b) and (d) are slightly biased by the loss of some N^{*++} events.[31] Correction for the loss has not been attempted because the decay distributions are generally flat and because the presence of four particles in the final state tends to smear out the biasing effect of the cuts. Furthermore, it is not generally feasible to do background subtractions for the N^{*++} channel because, as may be seen in Fig. 2(b), a control region of mostly background events is only available on the high side of the peak and is too far removed from the central resonant interval to justify its use.

The decay distributions for events in the backward N^{*++} spike, $\hat{N}^{*++} \cdot \hat{K}^-_{in} < -0.8$, are shown cross-hatched in Fig. 14(b), (d). They are consistent with isotropy except for the small asymmetry in $\cos\theta_{target}$. In contrast, unmodified pion exchange or magnetic dipole ρ exchange[32] in the diagram shown in Fig. 13(b) requires $1+3\cos^2\theta$ with respect to the target or normal directions, respectively. The possibility that the backward N^{*++} peak is due to a mixture of π and ρ exchange cannot, however, be ruled out. Further angular correlation studies, especially with regard to other diagrams for N^{*++} production, failed to yield additional evidence for a peripheral mechanism in reaction (10).

Next, the production and decay distributions of $Y^{*0}(1520)$ in the reaction

$$K^- + p \to Y^{*0} + \pi^+ + \pi^- \qquad (11)$$

---
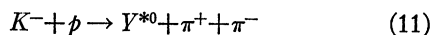
[31] On a Dalitz plot of $M(p\pi^+)$ versus $M(K^-\pi^+)$, for example, with $M(K^-p\pi^+)$ fixed, the cosine of N^{*++} decay with respect to its direction of motion in the $K^-p\pi^+$ frame varies linearly along the N^* mass band. Removing an interval of $M(K^-\pi^+)$ removes all the events in a section of that angular distribution. The effect is smeared out in our case because $M(K^-p\pi^+)$ is not fixed and because we are plotting the decay angle with respect to the target proton direction.

[32] L. Stodolsky and J. J. Sakurai, Phys. Rev. Letters **77**, 90 (1963).

are considered. The $Y^{*0}\rho$ reaction is below threshold. Y^* events were selected according to $1.50 < M(K^-p) < 1.54$ GeV, which yields a $\sim 48\%$ pure Y^* sample. Background due to $\bar{K}^*$ was reduced by removing events with $0.86 < M(K^-\pi^+) < 0.92$ GeV, resulting in a $\sim 55\%$ pure Y^* sample. The distribution of momentum transfer to the Y^{*0} is shown in Fig. 15(a). The decay distributions for each sample are shown in Fig. 16 and for events with low momentum transfer to the Y^* in Figs. 15(b) and (c). The data differ from the N^{*++} case in that the distribution of $\cos\theta_{target}$ for the Y^* [Fig. 16(b)] is markedly polar and forward-backward-symmetric. However, the polarity, which implies preferential population of the $m = \pm\frac{1}{2}$ substates of the Y^*, does not seem to be associated with K exchange [see the diagram in Fig. 15(a)], since the distribution is flat for low momentum transfer events as shown by Fig. 15(b).

The angular correlations for Y^{*0} production and decay have been compared to those obtained using control regions in K^-p mass below and above the Y^{*0} band. No significant variations were observed in this way, in agreement with the smooth behavior of the production moments of the K^-p system plotted in Fig. 8(d).

G. $\bar{K}^{*0}N^{*0}$ Production and Decay

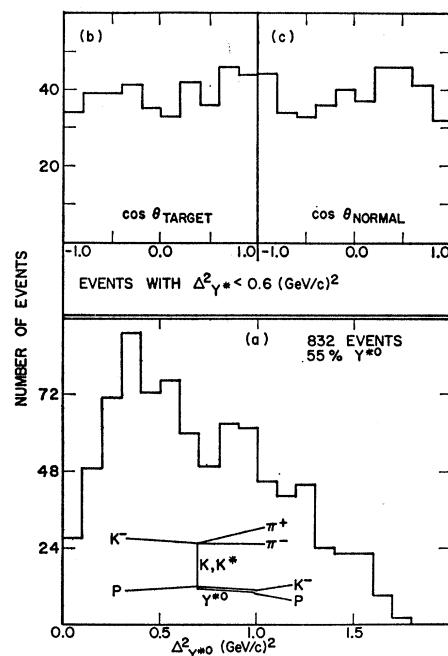According to the maximum-likelihood fit, 20% of the total or 900 events are pseudo-two-body events of

FIG. 15. (a) Distribution of momentum-transfer squared in the reaction $K^-p \to Y^{*0}(1520)\pi^+\pi^-$. The diagram shown is the one-meson-exchange diagram for which the Y^{*0} is produced alone at the lower vertex. Plots (b) and (c) show the decay distributions for events produced with low momentum transfer in this diagram, i.e., $\Delta^2 < 0.6$ $(\text{GeV}/c)^2$. The events plotted lie in the $Y^{*0}(1520)$ band but not in the $\bar{K}^*$ band.

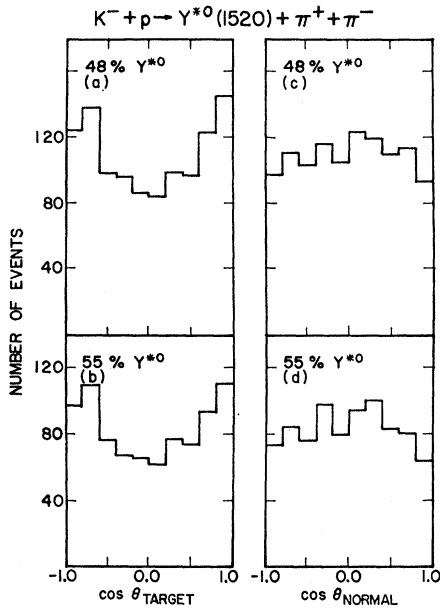$K^- + p \to Y^{*0}(1520) + \pi^+ + \pi^-$

FIG. 16. Decay angular distributions of the Y^{*0} system with respect to the target proton and normal $(\hat{K}^- \times \hat{Y}^{*0})$ directions. Plots (a) and (c) show events in the Y^{*0} mass band; events in the $\bar{K}^*$ band were removed in plotting (b) and (d).

the type $K^-p \to \bar{K}^{*0}N^{*0}$. Simultaneous K^*N^* production has been studied in both K^+p and K^-p interactions in the region of a few GeV/c incident momentum. The reaction $K^+p \to K^{*0}N^{*++}$ has been studied at 1.96, 3.0, and 3.5 GeV/c.[7-10] In each case, the experimenters found evidence for one-pion exchange, i.e., characteristic decay angular distributions and peaked production distributions.

At 1.96 GeV/c, the data showed strong correlation between the K^* and N^* decay.[8] This is inconsistent with pure pseudoscalar-meson exchange; the authors suggest final-state interactions or exchange of two pseudoscalar mesons as the explanation. Our reaction, $K^-p \to \bar{K}^{*0}N^{*0}$ has been studied at 3.0 GeV/c[33] and found to be both peripheral and dominated by one pion exchange at that energy. It is noteworthy that the K^*N^* reaction was quite cleanly separable in the K^+p experiments and that a clean ($\sim$15% background) sample of $\bar{K}^{*0}N^{*0}$ events could be obtained in K^-p at 3.0 GeV/c by selecting low-momentum transfer events.

Jackson et al.[34] have fit the $K^+p \to K^*N^*$ reaction at 3.0 and 3.5 GeV/c to a one-meson-exchange model with absorption effects included. They find good agreement between the experimental K^* and N^* density matrix elements and the model incorporating only pion exchange. However, inclusion of ρ exchange improves

[33] P. Schlein (private communication), based on work of Ecole Polytechnique-Saclay-Amsterdam collaboration on K^-p interactions at 3 GeV/c.

[34] J. D. Jackson, Rev. Mod. Phys. 37, 484 (1965); J. D. Jackson, J. T. Donohue, K. Gottfried, R. Kayser, and B. E. Y. Svensson, Phys. Rev. 139, B428 (1965).

the fit to the differential cross section. Destructive interference between the pion and ρ exchange also brings the predicted absolute cross sections into better agreement with experiment.

The assumption of K^*N^* production via exchange of a $T=1$ meson leads through the application of charge conjugation invariance at the boson vertex and charge independence at the baryon vertex to the relation for the total cross section,

$$\sigma(K^-p \to \bar{K}^{*0}N^{*0}) = \tfrac{1}{3}\sigma(K^+p \to K^{*0}N^{*++}). \quad (12)$$

After correction of the partial cross section given in Table II for the charge states of $\bar{K}^{*0}$ and N^{*0} which are not observed in this experiment, the value $\sigma = 0.57 \pm 0.06$ mb is obtained for the left-hand side of Eq. (12). Goldhaber et al.[7] report $\sigma = 1.1 \pm 0.2$ mb at $P_{K^+} = 1.96$ GeV/c for $K^+p \to K^{*0}N^{*++}$ with $K^{*0} \to K^+\pi^-$. Correction for $K^0\pi^0$ decay yields $(K^+p \to K^{*0}N^{*++}) = 1.6 \pm 0.3$ mb or 0.5 ± 0.1 mb for the right-hand side of Eq. (12) which is seen to be well satisfied experimentally assuming negligible variation of $\sigma(K^*N^*)$ between 1.96 and 2.0 GeV/c.

We now attempt further comparison of the 2.0-GeV/c $K^-p \to \bar{K}^*N^*$ data with the predictions of one-meson exchange. First of all, it is desirable to make a clean separation of the $\bar{K}^{*0}N^{*0}$ events and to understand the effects of the remaining background contamination. A glance at Figs. 2(a) and 3(b) indicates that even the minimum attainable background levels under the N^{*0} and $\bar{K}^{*0}$ peaks are $\gtrsim$30%. The separation of $\bar{K}^*N^*$ events was made on the basis of the joint Breit-Wigner weight of Eq. (7). Let $\alpha = |T_{K^*}|^2 \times |T_{N^*}|^2$, normalized so that $0 < \alpha \leqslant 1.0$. Alpha is then a convenient parameter for selecting K^*N^* events; α approaches unity near the center of the K^*N^* "spot" on the scatter plot of Fig. 7 and approaches zero far away from this region. Curves of constant α are approximately elliptical in shape and provide a cleaner separation than could be achieved by merely defining bands of $K^-\pi^+$ and $p\pi^-$ mass. For the purposes of plotting angular distributions and doing background subtractions, two intervals of α were chosen and the percentage of $\bar{K}^*N^*$ and background events in these intervals was determined from the Monte-Carlo events. The region $1.0 \geqslant \alpha > 0.2$ contains approximately 55% $\bar{K}^*N^*$ and 45% non-$\bar{K}^*N^*$ events; 70% of all doubly resonant events are included. The "background" interval, $0.2 \geqslant \alpha > 0.02$, contains 20% $\bar{K}^*N^*$ and includes 26% of the doubly resonant events.

A sample containing as large a fraction as 70% $\bar{K}^*N^*$ events can be obtained by selecting a sufficiently small region of α, but only about 10% of the doubly resonant events would be included. Furthermore, selection of events in which the N^{*0} is produced in the backward direction does not significantly improve the purity of the sample. The distribution of production-angle cosine of the $p\pi^-$ (N^{*0}) system is shown in Figs. 17(a) and (b) for the regions of α defined above. The ratio of events
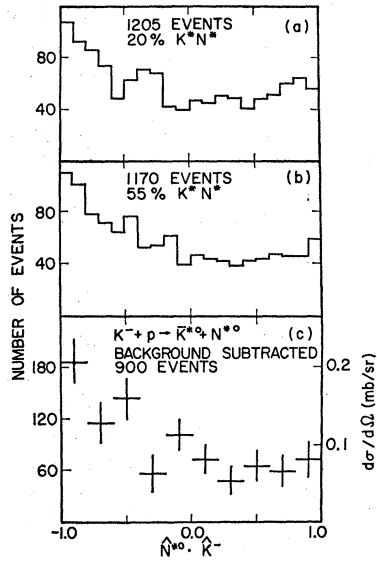
FIG. 17. Production angular distribution of N^{*0} in the reaction $K^-p \to \bar{K}^{*0}N^{*0}$. Plot (a) shows the events satisfying $0.2 \geqslant \alpha > 0.02$, approximately 20% of which are $\bar{K}^*N^*$ events; plot (b) shows the events satisfying $1.0 \leqslant \alpha > 0.2$, approximately 55% of which are $\bar{K}^*N^*$ events. Plot (c) shows the result of subtracting the "background" plot (a) from the mostly resonant plot (b).

in the backward hemisphere to those in the forward is 1.36 in case (a) (mostly background) and 1.57 in case (b) (mostly $\bar{K}^*N^*$). Figure 17(c) shows the result of a simple background subtraction applied to plots (a) and (b); the backward to forward ratio of the resulting resonant distribution is 1.91. The background subtraction indicates that the peripheral selection $-1.0 \leqslant \hat{N}^*$-
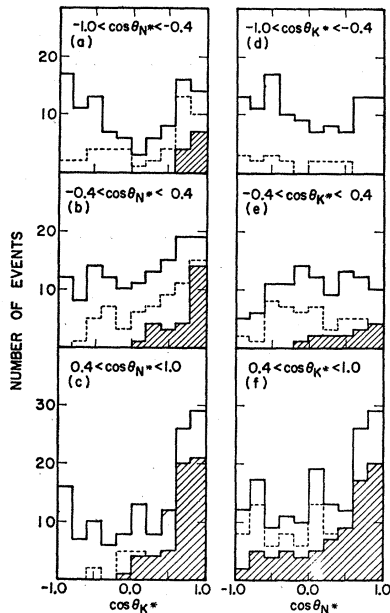

FIG. 18. Decay angular distributions of the $\bar{K}^{*0}$ and N^{*0} systems with respect to the beam and target proton directions, respectively, in the reaction $K^-p \to \bar{K}^{*0}N^{*0}$. The events plotted satisfy $1.0 \geqslant \alpha > 0.2$ and squared-four-momentum transfer to the $\bar{K}^{*0}$, $\Delta^2 < 0.5$ $(\text{GeV}/c)^2$. Plots (a), (b), and (c) show $\cos\theta_{K^*}$ for backward, equatorial, and forward intervals of the N^{*0} decay. Plots (d), (e), and (f) show $\cos\theta_{N^*}$ for intervals of $\cos\theta_{K^*}$. The events plotted in the dashed histograms also lie in the N^{*++} band, $1.13 < M(p\pi^+) < 1.27$ GeV, while those in the cross-hatched histograms satisfy $\hat{N}^{*++} \cdot \hat{K}^- < -0.7$ as well.

$\cdot \hat{K}^- < -0.6$ provides an increase of only 5% in the fraction of $\bar{K}^*N^*$ events in the interval $1.0 \geqslant \alpha > 0.2$.

Thus a clean sample of $\bar{K}^*N^*$ events cannot be obtained in our experiment. The large background contamination seriously distorts the decay distributions. The largest contributor to this background is the N^{*++} production channel; its effect on the $\bar{K}^{*0}$ and N^{*0} decay distributions is shown in Fig. 18. "T-channel" coordinates are used, so that the polar decay angle, θ_{K^*}, is the angle between incident and outgoing K^- in the $\bar{K}^*$ rest frame. Similarly, θ_{N^*} is defined as the angle between the target and outgoing protons. The events plotted in Fig. 18, approximately 60% of which are $\bar{K}^*N^*$, satisfy $1.0 \geqslant \alpha > 0.2$ and have low squared four^0 momentum transfer to the $\bar{K}^{*0}$, $-t = \Delta^2 < 0.5$ $(\text{GeV}/c)^2$. Distributions of $\cos\theta_{K^*}$ and $\cos\theta_{N^*}$ are shown for backward, equatorial, and forward intervals of the other cosine. Plots (c) and (f) are asymmetric; each displays a pronounced forward decay peak. Asymmetry is illegal by angular momentum and parity conservation in the strong decay of a free particle. However, these peaks are largely accounted for by events with a $p\pi^+$ system produced backwards and with mass in the N^{*++} band, as shown by the dashed $[1.13 < M(p\pi^+) < 1.27$ GeV$]$ and cross-hatched $(\hat{N}^{*++} \cdot \hat{K}^-_{\text{in}} < -0.7)$ histograms in Fig. 18. As noted above, there is a prominent backward peak in the N^{*++} production angular distribution [Fig. 13(a)] which persists for $K^-\pi^+$ masses both inside and outside the $\bar{K}^*$ band. Events with a backward $p\pi^+$ system of low $(\sim M_{N^*})$ mass overlap kinematically with forward decays of forward-produced $\bar{K}^*$'s. Events in the overlap region also tend to have forward "N^{*0}" decays (with respect to the target proton). Thus, the strong backward peak in N^{*++} production results in asymmetric $\bar{K}^{*0}$ and N^{*0} decay distributions, especially when forward $\bar{K}^*$ events are selected.

To summarize, the large background contamination in the $\bar{K}^{*0}N^{*0}$ event sample prevents meaningful comparison of the angular correlations with the peripheral model. The observed decay distributions are not characteristic of either simple π or ρ exchange. In addition, the production angular distribution is not highly peaked backward, which is not very surprising in view of the lack of available kinetic energy (only about 125 MeV for average $\bar{K}^*$ and N^* masses). However, the comparison of the total cross sections for K^*N^* production in K^-p and K^+p scattering is consistent with dominance by $T=1$ meson exchange, a result which also obtains at 3.0 GeV/c.[38]

IV. CONCLUSION

At 2 GeV/c the situation in the $K^-p\pi^+\pi^-$ final state appears to be quite complicated. The final state is dominated by resonance production in at least seven channels. Unfortunately, the low available kinetic energy, the production of broad N^* resonances in at least 75% of the events, and the kinematic overlaps of

the many channels conspire to prevent a clean separation of the various reactions. The optimum background levels which can be obtained by mass and momentum transfer selections vary from 25 to 75%. The two- and three-body channels are not dominantly peripheral; decay distributions characteristic of resonance production via single meson exchange are not observed in any of the channels. The production rates of the resonant channels are all of the same order of magnitude when detection and phase-space factors are taken into account; this fact may be a reflection of the complexity of the situation.

Experimental Limit for the Neutron Charge*

C. G. Shull, K. W. Billman, and F. A. Wedgwood†

Massachusetts Institute of Technology, Cambridge, Massachusetts

(Received 25 August 1966)

A microscopic measurement of the charge on a free, monoenergetic neutron has led to the value of $(-1.9\pm3.7)\times10^{-18}$ electron charges. This is consistent with the usual view that neutrons are electrically neutral. The experiment has exploited the very high angular sensitivity of a double-crystal spectrometer in assessing the angular deflection of a monoenergetic neutron beam under electrostatic deflection conditions. An improvement of about six orders of magnitude in the upper limit of the charge over previously published values obtained by direct experimentation has been attained.

INTRODUCTION

ACCORDING to present views, the neutron is thought to be an electrically neutral particle. In this paper an experimental test for a minute charge is described in which the angular deviation of a monoenergetic neutron beam under the action of a homogeneous transverse deflecting field is sensed. The absence of such a deflection, coupled with the calibrated sensitivity of the apparatus, confirms the belief of neutron neutrality.

The search for a neutron charge is important in the information it may provide for fundamental-particle theory. Here the charge and mass remain as yet empirical values which theory cannot predict. Indeed, any experiment is of interest which may shed light on the apparent property of all particles to bear integral multiples of the electron charge. The present measurement may be construed as the most precise charge measurement of an elementary particle, and thus sets a severe criterion to be met by any future theory.

In an interesting paper, Feinberg and Goldhaber[1] discuss the necessity and implications of setting accurate experimental limits on the charges of elementary particles. The present belief that the conservation laws of charge, baryon number, and lepton number are independent and absolute leads to the conclusion that known particle processes can only determine the relative magnitudes of charges. Experimental limits on, for example, the neutron charge and the electron-proton charge difference are thus essential. Furthermore, if it were found that the charges of the baryons were all slightly different from their commonly accepted values by a common amount, then the conservation of baryons would follow from the conservation of charge rather than being an independent principle. Similar remarks hold for leptons.

Turning from microscopic to macroscopic considerations, much speculation about the cosmological consequence of a finite electron-proton charge difference, $\Delta q = |q_e| - |q_p|$, has been made. If one assumes charge conservation to hold in the neutron-decay process $n \to p + e^- + \bar{\nu}$, then Δq is equal to the neutron charge q_n upon the further assumption that the neutrino is

---

[1] G. Feinberg and M. Goldhaber, Proc. Natl. Acad. Sci. U. S., **45**, 1301 (1959); also M. Gell-Mann, in *Proceedings of the 1960 Annual International Conference on High-Energy Physics at Rochester* (Interscience Publishers, Inc., New York, 1960), p. 792.